VIMO: VITAL SIGN MONITORING USING COMMODITY MILLIMETER WAVE RADIO

Fengyu Wang, Feng Zhang, Chenshu Wu, Beibei Wang and K. J. Ray Liu

University of Maryland, College Park, MD 20742, USA
Origin Wireless Inc., Greenbelt, MD 20770, USA

ABSTRACT

Accurate monitoring of human vital signs (e.g. breathing and heart rates) is crucial in detecting medical problems. In this paper, we propose **ViMo**, a calibration-free remote **Vi**tal sign **Mo**nitoring system that can simultaneously monitor multiple users by leveraging the channel impulse response (CIR) of 60GHz WiFi. By exploiting the periodicity introduced by respiration, we first propose a human detection algorithm which does not require any prior calibration. Then, we apply the auto-correlation function (ACF) of the CIR phase to estimate the breathing rate. Lastly, to mitigate the impact of the breathing signal on the weak heartbeat signal, the cubic spline interpolation is used to eliminate the breathing signal before the estimation of the heart rate. Extensive experiments show that ViMo can achieve a median accuracy of 0.19 BPM for breathing rate estimation and 1 BPM for heart rate estimation, outperforming the existing non-contact solutions that are purely based on frequency analysis.

***Index Terms*—** Vital signs monitoring, 60GHz WiFi, channel impulse response (CIR), cubic spline interpolation.

1. INTRODUCTION

Vital signs such as breathing and heartbeat play a crucial role to evaluate an individual's health status. Most conventional vital sign monitoring methods require physical contact, which is not convenient for daily use.

With the ubiquitous deployment of WiFi devices, recent research has considered to use WiFi signals for vital sign estimation [1, 2]. However, the capability of the 2.4/5GHz WiFi system is fundamentally limited by the narrow bandwidth, small antenna number, and large wavelength. Specifically, due to the small number of antennas, the spatial resolution of these systems is too low to distinguish the RF signals reflected by multiple users [3–7]. Furthermore, the large wavelength and multiple reflections from indoor objects make it difficult to observe the subtle change caused by heartbeat.

The emerging of 60GHz WiFi (e.g., 802.11ad [8]) brings new opportunities to the RF-based vital sign monitoring. mmVital proposed in [9] shows the possibility of utilizing the received signal strength (RSS) of 60GHz millimeter-wave to do vital sign monitoring. However, the system needs to be calibrated first to eliminate the influence introduced by the environment. Furthermore, the extra mechanical cost is introduced to change the antenna direction of horn antennas.

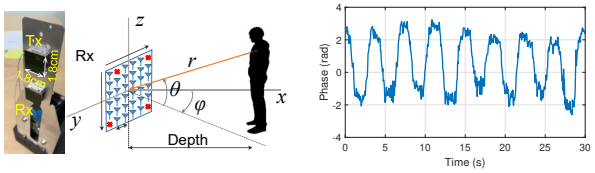

(a) Device and coordinate system (b) Typical phase signal with vital sign

Fig. 1: Coordinate system and typical signal

In this work, we develop ViMo, a **Vi**tal sign **Mo**nitoring system using commercial 60GHz WiFi. We utilize the fine-grained channel impulse response (CIR) to detect vital signs. The key contributions of the paper are summarized as below.

- We build a theoretical model of the CIR with the existence of multiple vital signs.
- A calibration-free human detection approach is proposed by leveraging large reflection strength of human subjects as well as periodicity introduced by vital signs.
- A novel method based on cubic spline interpolation is introduced to remove respiration signals for heart rate estimation.

The rest of the paper is organized as follows. Section 2 presents the theoretical model of CIR with the influence of vital signs. The details of the design are introduced in Section 3 and the experimental evaluation is discussed in Section 4. Section 5 concludes the paper.

2. THEORETICAL MODELING OF CIR MEASUREMENTS

As shown in Fig. 1 (a), we use commodity Qualcomm 60GHz chipsets, where the device operates in radar mode when monitoring vital signs. The device has 32 elements assembled in a 6×6 layout for both the transmitter (Tx) and the receiver (Rx) and operates at 60GHz center frequency with 3.52GHz bandwidth. The Tx transmits a known pulse sequence for channel impulse response (CIR) estimation.

Assume the traveled distance of the electromagnetic (EM) wave reflected by human chest is $d(t)$, then the CIR between Tx antenna m and Rx antenna n can be expressed as

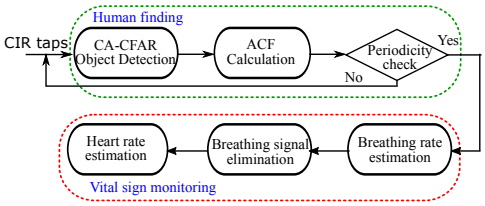

Fig. 2: Processing flow of ViMo

$$h_{m,n}(t) = a_{m,n}(t)\exp(-j2\pi\frac{d_{m,n}(t)}{\lambda_c}), \tag{1}$$

where $a_{m,n}(t)$ is the complex channel gain, λ_c denotes the wavelength of the carrier. Due to the modulation of the vital signs, i.e., respiration and heartbeat, $d_{m,n}(t)$ appears to be a combination of two periodic signals, which can be further expressed as

$$d_{m,n}(t) = d_0(m,n) + s_r(t) + s_h(t), \tag{2}$$

where $s_r(t)$ and $s_h(t)$ denotes the distance change due to respiration and heartbeat. Besides, $d_0(m,n) = lT_sc + \Delta d(m,n)$, where $T_s = 1/B$ denotes the fast time resolution and B stands for the system bandwidth. Here we assume the reflected signal falls into the l-th tap of the measured CIR with residual $\Delta d(m,n)$, then the l-th tap of the CIR, $\mathbf{h}_l(t) = [h_{1,1}(t), h_{1,2}(t), \ldots, h_{M,N}(t)]^T$ can be expressed as

$$\begin{aligned}\mathbf{h}_l(t) &= \mathbf{a}(t) \odot \exp(-j2\pi\frac{\mathbf{d}_0 + s_r(t) + s_h(t)}{\lambda_c}) \\ &= \tilde{\mathbf{a}}\exp(-j2\pi\frac{s_r(t) + s_h(t)}{\lambda_c}),\end{aligned} \tag{3}$$

where $\mathbf{d}_0 = [d_0(1,1), d_0(1,2), \ldots, d_0(M,N)]^T$, $\mathbf{a}(t) = [a_{1,1}(t), a_{1,2}(t), \ldots, a_{M,N}(t)]^T$, and $\odot$ denotes elementwise product. We assume $\mathbf{a}(t)$ is time-invariant due to the tiny movement of the subject, and the common phase shift is absorbed in the term $\tilde{\mathbf{a}}$. The CIR after performing beamforming can be expressed as

$$h_{\theta,\phi}(t) = \mathbf{s}^H(\theta,\phi)\mathbf{h}_l(t) + \epsilon(t), \tag{4}$$

where $\mathbf{s}(\theta,\phi)$ is the steering vector pointing to the direction (θ,ϕ) and $\epsilon(t)$ stands for additive white Gaussian noise which are independent and identically distributed (I.I.D) for different links. It is apparent that the phase of the CIR measurement changes periodically in slow time due to the periodic motions of respiration and heartbeat, as shown in (3). Fig. 1 (b) shows a typical phase signal containing vital signs collected by our system.

3. DESIGN OF VIMO

The workflow of ViMo consists of two main steps, i.e., **human finding** and **vital sign monitoring**, as shown in Fig.2. The details will be discussed in the following subsections.

3.1. Object detection

Since various indoor objects (e.g., wall, desk, etc.) reflect the EM wave, before starting monitoring vital signs, we first need to detect human subjects in the vicinity of the Tx and the Rx. The CIR measurement for the case when there is no reflecting object and the case when there is a static reflecting object on a certain tap can be expressed as,

$$h^{\text{empty}}_{\theta,\phi}(t) = \epsilon(t), \tag{5}$$

and

$$h^{\text{static}}_{\theta,\phi}(t) = \mathbf{s}^H(\theta,\phi)[\mathbf{a} \odot \exp(-j2\pi\frac{\mathbf{d}_0}{\lambda_c})] + \epsilon(t), \tag{6}$$

respectively. It is obvious that the power response when there is a reflecting object is much larger than the empty tap. Besides, for the same reflecting object, a shorter distance corresponds to a larger power gain. Therefore, we can use thresholding on the power response to determine if a reflecting object exists and the threshold for the power response should be adaptive to the distance between the device and the subject.

In our system, a cell-averaging constant false alarm rate (CA-CFAR) [10] algorithm is adopted to detect human presence. Specifically, the threshold level is calculated by estimating the level of the noise floor around the cell under test (CUT). Furthermore, the guard cell is used to avoid corrupting estimates with power from the CUT itself. By applying CA-CFAR, we can find the candidate taps which are affected by reflecting objects. Observe that the tap affected by chest movement will exhibit a periodic phase according to (3) while the tap affected by the static reflector does not, we will determine the final estimate of human location by considering the periodicity property, which will be discussed in Section 3.2.

3.2. Breathing rate estimation

Observing that the breathing signal is periodic, spectrum analysis can be used to estimate the respiration rate [11]. However, the frequency resolution is $\Delta f = \frac{1}{W}$ breath per minute (BPM), where W is the window length in seconds. Therefore, to get an acceptable estimation accuracy, the window length should be long enough, which will cause a large delay. In our system, we adopt a statistical approach by examining the auto-correlation function (ACF) of the candidate CIR phase. Here we denote the time-variant part of CIR phase measurement as

$$x(t) = s_r(t) + s_h(t) + n(t), \tag{7}$$

where $n(t)$ is the random phase offset introduced by noise, and is also a random variable independent in time instances. Thus the ACF of $x(t)$ can be calculated as

$$\rho(\tau) = \frac{cov[x(t), x(t+\tau)]}{cov[x(t), x(t)]}, \tag{8}$$

where τ denotes the time lag, and $cov[\cdot]$ denotes the convariance operator. Assume that the distance change caused

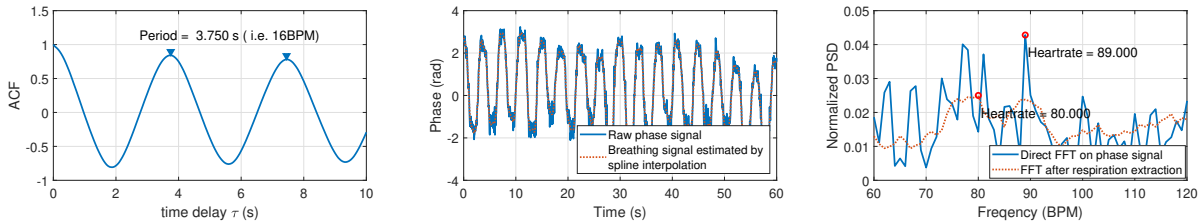

(a) ACF of phase signal (b) Breathing signal elimination (c) Spectrum for the heartbeat signal

Fig. 3: Example of vital sign monitoring. The subject has a breathing rate of 16 BPM and a heart rate of 80 BPM.

by heartbeat $s_h(t)$ is uncorrelated with the distance change caused by respiration $s_r(t)$, then $\rho(\tau)$ can be expressed as

$$\rho(\tau) = \frac{var[s_r(t)]}{var[x(t)]}\rho_r(\tau) + \frac{var[s_h(t)]}{var[x(t)]}\rho_h(\tau) + \frac{var[n(t)]}{var[x(t)]}\rho_n(\tau), \tag{9}$$

where $var[x(t)] = var[s_r(t)] + var[s_h(t)] + var[n(t)]$, and $var[\cdot]$ denotes the variance operator. $\rho_r(\tau), \rho_h(\tau)$ and $\rho_n(\tau)$ denote the ACF of respiration, heartbeat and noise respectively. Since we have $var[s_r(t)] \gg var[s_h(t)]$ and $var[s_r(t)] \gg var[n(t)]$, then we have the approximation that $\rho(\tau) \approx \rho_r(\tau)$. The ACF will have a definite peak at a certain delay which corresponds to the breathing cycle as shown in Fig. 3 (a). ACF analysis will be adopted to the candidate cells in CA-CFAR to eliminate the static objects, and thus we can locate human subjects.

3.3. Heart rate estimation

Heartbeat can introduce minute movements of the chest, which can be detected as small peaks in the unwrapped phase as shown in Fig. 1 (b). Past works [9,12,13] try to directly utilize frequency analysis and bandpass filter (BPF) to estimate the heart rate. However, due to the harmonics introduced by respiration, it is easy to pick up the wrong peak for estimation as shown in Fig. 3 (c). To eliminate the impact caused by respiration, the polynomial fitting has been used [14, 15] to remove respiration motion. However, one of the main drawbacks of the polynomial fitting is the order selection. In the previous work, the order is just selected by empirical experience, which can easily cause under-fitting or over-fitting when the experimental setting is changed.

In this work, we utilize cubic spline interpolation [16], which can effectively remove the respiration while keeping the heartbeat motion as shown in Fig. 3 (b), and then the heart rate can be easily estimated by performing a *fast Fourier transform* (FFT). The spectrum of the residue after the elimination of the breathing signal is shown in Fig. 3 (c), and it can be easily seen that the harmonics of breathing has been effectively suppressed.

4. EXPERIMENT EVALUATION

In this section, we evaluate ViMo in practical settings using a commodity 802.11ad chipset in a typical office of size $3.5\ \mathrm{m} \times 3.2\ \mathrm{m}$. We enroll 8 participants (4 male and 4 female) aging from 22 to 35 for testing. The ground truth is provided by a commercial sensor with a chest strap [17].

4.1. Impact of distance

In this section, we investigate the effect of the distance between the device and human subject on the estimation accuracy. Experiment participants sit at different places facing the device. Fig. 4 (a) and Fig. 5 (a) illustrate the empirical cumulative distribution function (CDF) of the absolute breathing and heart rate error. To account for the miss-detection, we set the estimation to be 0 BPM when the target is missed. Besides, since the resolution of our estimation for breathing is 0.05 BPM, and the ground truth and estimation for heart rate are both 1 beat/minute (BPM), the CDFs appear to be stepwise.

As expected, the performance degrades with distance due to the signal to noise ratio (SNR) degradation. Furthermore, we can see that the degradation of breathing rate estimation is less than the heart rate estimation. This is because the breathing signal is much stronger than the heartbeat signal, which corresponds to higher SNR. The median estimation error for respiration rate and heart rate are within 0.19 BPM and 1 BPM respectively when the distance is within 1.5 m. They raise to 0.22 BPM and 2 BPM when the distance increases to 2 m.

4.2. Impact of orientation

In this study, the orientation corresponds to the closest part of the user w.r.t the device. The distance from the user to device is set to be 1 m. Fig. 4 (b) and Fig. 5 (b) show the effect of user orientation. We can see that the equivalent performance of heart rate estimation can be achieved with "front" and "left" settings, outperforming than the "right" and "back" settings. This is due to the physiological structure of human beings, where the vibration caused by the heartbeat is larger on the left side of the chest. However, the inhale and exhale will

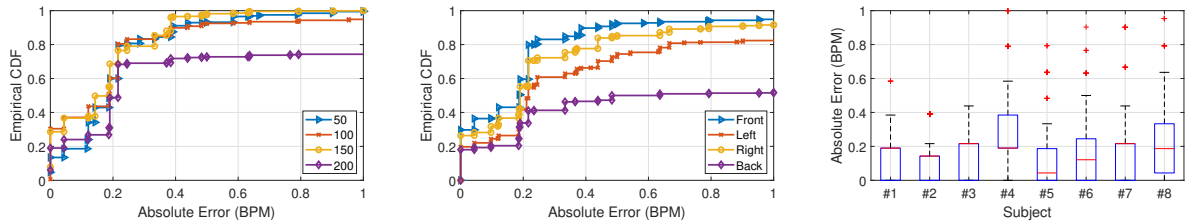

(a) The impact of distance (b) The impact of orientation (c) The impact of user heterogeneity

Fig. 4: Performance of respiration rate estimation. ViMo estimates w.r.t. (a) the distance (b) the orientation (c) different users

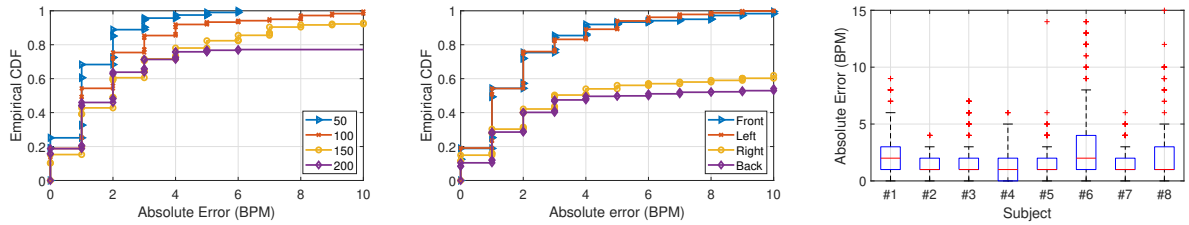

(a) The impact of distance (b) The impact of orientation (c) The impact of user heterogeneity

Fig. 5: Performance of heart rate estimation. ViMo estimates w.r.t. (a) the distance (b) the orientation (c) different users

cause the whole chest move up and down, so for the respiration rate, execpt for the "back" case, all the other orientations have similar performance.

4.3. Impact of user heterogeneity

In this part, we investigate the impact of the user heterogeneity on the performance. The difference in error distribution can be caused by various factors, such as reflection loss and heartbeat strength, etc. Fig. 4 (c) gives the respiration rate estimation performance, with the maximum median error within 0.2 BPM for all volunteers. Fig. 5 (c) shows the error distribution of absolute heart rate error of all 8 subjects, where all of them have a median error within 2 BPM.

4.4. Multi-user case

In this part, we study the impact of angle separation between multiple users, where two users sit at a distance of 1 m away from the device with different separation angles. We define the detection index (DI) of a separation angle as the ratio between the number of samples when the number of detected targets matches the ground truth and the total number of samples. We also define the false-alarm index (FI) of a separation angle as the ratio between the number of samples when the number of detected targets is larger than the ground truth and the total number of samples. We also give the median error of breathing rate and heart rate estimation for both users. The results are summarized in Tab. 1.

Compared to the single-user scenario, the performance degrades at small separation angles, but the performance is similar for different separation angles if the angels are large enough. This is because that when the distance of two targets is small enough, the distance of the candidate cells in CA-CFAR associated with each user can be smaller than the predefined threshold. Thus, there will be only one representative cell left, resulting in a miss detection. Also, the high SNR cells of one user can be merged with the other user's, therefore, the SNR of the representative cell for vital signs estimation can drop, resulting in degradation of the performance.

Separation angle	DI	FI	Med. error of breathing	Med. error of heart rate
30°	0.87	0	(0.21;0.97)	(1;1)
45°	0.96	0	(0.63;0.21)	(3;1)
60°	1	0	(0.22;0.21)	(1;1)
75°	1	0	(0.22;0.28)	(1;1)

Table 1: Performance for different separation angles

5. CONCLUSION

In this paper, we develop ViMo to track human vital signs using CIR measured by 60GHz commercial WiFi chips. We design a human detection algorithm without calibration by leveraging periodicity introduced by respiration. Cubic spline interpolation is further introduced to eliminate the interference of breathing signals on heart rate estimation. Experiment results show the potential of the proposed system for contactless human vital sign monitoring with high accuracy.

6. REFERENCES

[1] K.J.R. Liu and B. Wang, *Wireless AI: Wireless Sensing, Positioning, IoT, and Communications*, Cambridge University Press, 2019.

[2] B. Wang, Q. Xu, C. Chen, F. Zhang, and K. J. R. Liu, "The promise of radio analytics: A future paradigm of wireless positioning, tracking, and sensing," *IEEE Signal Processing Magazine*, 2018.

[3] F. Zhang, C. Wu, B. Wang, M. Wu, D. Bugos, H. Zhang, and K. J. R. Liu, "SMARS: Sleep monitoring via ambient radio signals," *IEEE Transactions on Mobile Computing*, 2019.

[4] C. Chen, Y. Han, Y. Chen, H. Lai, F. Zhang, B. Wang, and K. J. R. Liu, "TR-BREATH: Time-reversal breathing rate estimation and detection," *IEEE Transactions on Biomedical Engineering*, 2018.

[5] C. Chen, Y. Han, Y. Chen, and K. J. R. Liu, "Multi-person breathing rate estimation using time-reversal on WiFi platforms," in *IEEE Global Conference on Signal and Information Processing (GlobalSIP)*, 2016.

[6] D. Zhang, Y. Hu, Y. Chen, and B. Zeng, "Breathtrack: Tracking indoor human breath status via commodity WiFi," *IEEE Internet of Things Journal*, 2019.

[7] J. Liu, Y. Chen, Y. Wang, X. Chen, J. Cheng, and J. Yang, "Monitoring vital signs and postures during sleep using WiFi signals," *IEEE Internet of Things Journal*, 2018.

[8] Qualcmm 802.11ad 60GHz WiFi, `https://www.qualcomm.com/products/features/80211ad`.

[9] Zhicheng Yang, Parth H. Pathak, Yunze Zeng, Xixi Liran, and Prasant Mohapatra, "Monitoring vital signs using millimeter wave," in *Proceedings of the 17th ACM International Symposium on Mobile Ad Hoc Networking and Computing*, 2016.

[10] M.A. Richards, *Fundamentals of Radar Signal Processing, Second Edition*, McGraw-Hill Education, 2014.

[11] L. Ren, H. Wang, K. Naishadham, O. Kilic, and A. E. Fathy, "Phase-based methods for heart rate detection using UWB impulse doppler radar," *IEEE Transactions on Microwave Theory and Techniques*, 2016.

[12] Fadel Adib, Hongzi Mao, Zachary Kabelac, Dina Katabi, and Robert C. Miller, "Smart homes that monitor breathing and heart rate," in *Proceedings of the 33rd Annual ACM Conference on Human Factors in Computing Systems*, 2015.

[13] S. Bakhtiari, T. W. Elmer, N. M. Cox, N. Gopalsami, A. C. Raptis, S. Liao, I. Mikhelson, and A. V. Sahakian, "Compact millimeter-wave sensor for remote monitoring of vital signs," *IEEE Transactions on Instrumentation and Measurement*, 2012.

[14] T. Ohtsuki and E. Mogi, "Heartbeat detection with doppler radar based on estimation of average R-R interval using viterbi algorithm," in *IEEE 27th Annual International Symposium on Personal, Indoor, and Mobile Radio Communications (PIMRC)*, 2016.

[15] Q. Lv, L. Chen, K. An, J. Wang, H. Li, D. Ye, J. Huangfu, C. Li, and L. Ran, "Doppler vital signs detection in the presence of large-scale random body movements," *IEEE Transactions on Microwave Theory and Techniques*, 2018.

[16] Carl d. Boor, *A Practical Guide to Splines*, Springer Verlag, 1978.

[17] Polar H10 heart rate monitors, `https://www.polar.com/us-en/products/accessories/h10_heart_rate_sensor`.